ACS APPLIED NANO MATERIALS

www.acsanm.org Article

Hydrogen-Controlled Spin Reorientation Transition in a Nanometer-Thick FePd Layer on Co/[Pt/Co]$_4$/Pt Multilayers for Applications in Spintronics

Kun-Jen Hsueh, Po-Chun Chang, Li-Jie Liaw, Alltrin Dhanarajagopal, Minn-Tsong Lin,* and Wen-Chin Lin*

Cite This: *ACS Appl. Nano Mater.* 2023, 6, 2784−2790 Read Online

ACCESS | Metrics & More | Article Recommendations

ABSTRACT: In this study, we deposited a hydrogen-sensitive FePd alloy film on Co/[Pt/Co]$_4$/Pt multilayers with perpendicular magnetic anisotropy (PMA). Through hydrogenation, spin-reorientation transition (SRT) from a perpendicular to an in-plane direction was observed in the 2-nm-thick FePd capped multilayer. Magneto-optic Kerr effect measurements were performed in hydrogen gas at pressures ranging from a vacuum of 5×10^{-3} mbar to H_2 gas at 200 mbar. Reversible SRT was demonstrated with the cyclic change of H_2 pressure. Furthermore, tuning the strength of the PMA multilayer by adjusting the thickness of the Pt layer changed the SRT-critical thickness of the FePd cap and the hydrogen-induced SRT behavior. These findings will be valuable for application in spintronics through the electronic control of H-migration.

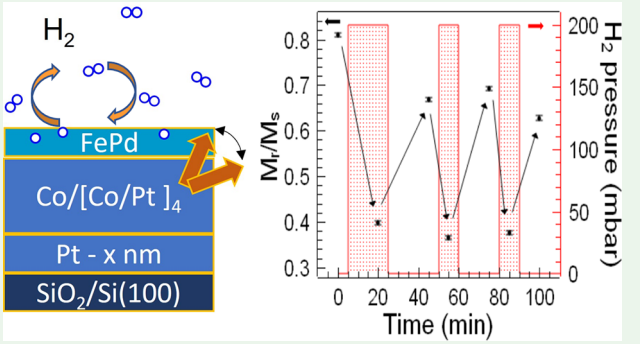

KEYWORDS: *magnetic thin film, multilayer, perpendicular magnetic anisotropy, hydrogen absorption, spin reorientation transition*

INTRODUCTION

Spin−orbit torque magnetic random access memory (SOT-MRAM) devices are considered promising candidates for use in next-generation nonvolatile memory devices due to their low power consumption, fast read/write speeds, and endurance ability.[1−4] However, the deterministic switching of perpendicular magnetization by spin−orbit torque (SOT) through the injection of in-plane polarized spin usually requires an additional in-plane external magnetic field to disrupt the symmetry of the perpendicular magnetic anisotropy (PMA). Considering the disadvantages of applying an external magnetic field, which requires complicated circuitry and additional power consumption, a field-free SOT switching mechanism should be developed. Numerous efforts have been made to realize field-free SOT switching mechanisms, including achieving lateral structural asymmetry using a wedge-layer,[5−7] voltage control in a multiferroic composite,[8] exchange-bias and interlayer exchange coupling,[9] and current-induced field-free switching.[10] Recently, Hwang et al. demonstrated the deterministic field-free SOT switching of perpendicular magnetization in amorphous and ferrimagnetic Gd/Co multilayers accompanied by a tilted magnetic anisotropy (TMA) axis, disrupting the symmetry of the PMA in a controlled manner, and providing an opportunity for switching perpendicular magnetization by using tilted anisotropy.[11]

In this experiment, we demonstrated the field-free reorientation of TMA films at room temperature in FePd/Co/[Pt/Co]$_4$/Pt multilayer structures grown on a SiO_2 substrate by the introduction of a hydrogenation effect.[12] Due to the high affinity of Pd to hydrogen gas, the magnetic properties of Pd-based magnetic alloys can be reversed by hydrogen, providing a strategy for controlling the PMA.[13] Accordingly, hydrogen-sensitive $Fe_{40}Pd_{60}$ alloys were used as the capping layer on Co/Pt-PMA multilayers. Despite their intrinsic in-plane magnetic anisotropy (IMA), the FePd alloy films exhibited PMA behavior induced by the magnetic proximity effect (MPE) resulting from proximity to Co/Pt multilayers. Thus, TMA films were fabricated by controlling the thickness of the FePd film and the buffer Pt film, and hydrogen-induced further tilting of the magnetic moment was

Received: December 1, 2022
Accepted: January 24, 2023
Published: February 6, 2023

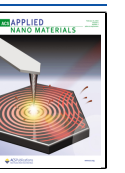

https://doi.org/10.1021/acsanm.2c05095
ACS Appl. Nano Mater. 2023, 6, 2784−2790

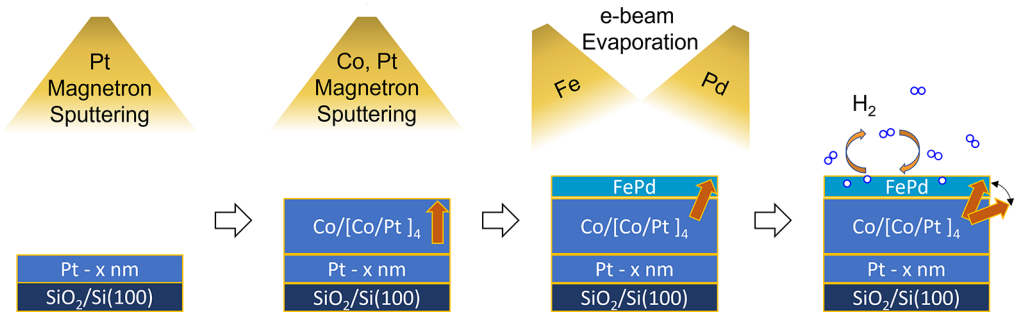

Figure 1. Schematic illustrations for the sample structure, fabrication processes, and hydrogen absorption-induced changes in magnetism.

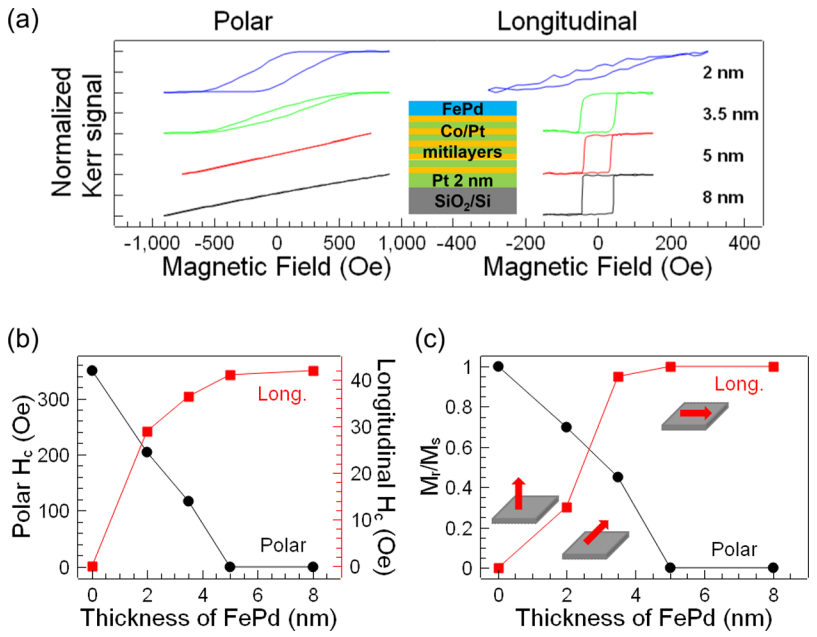

Figure 2. (a) Polar and longitudinal MOKE hysteresis loops with variation of FePd thickness. For clear exhibition, the saturation Kerr signal was normalized. (b) Magnetic coercivity (H_c), (c) the remanence to saturation magnetization (M_r/M_s) ratio of polar (black) and longitudinal (red) Kerr signals are plotted as a function of FePd thickness.

observed. In summary, this work provides new possibilities for performing the promising spin-reorientation transition (SRT) of the perpendicular magnetization in TMA films. In a real solid-state device, the SRT could be triggered by voltage-gated ion transport. For example, the reversible toggling of MAE using a small gate voltage through H^+ pumping in all-solid-state heterostructures has been demonstrated by Tan el al.[14]

EXPERIMENTAL SECTION

PMA multilayer thin films, composed of Co(0.3 nm)/[Pt(0.8 nm)/Co(0.3 nm)]$_4$/Pt(1−8 nm), were fabricated through magnetron sputtering in argon atmosphere, as illustrated in Figure 1. The Pt target was sputtered at 10 W dc, and the Co target was sputtered at 20 W dc. The sputtering rate of Co was 0.3 nm/min, and the sputtering rate of Pt was 2.5 nm/min. A base pressure of 1×10^{-8} Torr was attained before sputtering, and Ar pressure was maintained at 6 mTorr during deposition.[15] No specific substrate cooling or heating was applied during the sputtering process. The $Fe_{40}Pd_{60}$ (FePd) alloy thin films were subsequently deposited on the PMA layers by using the coevaporation method with two e-beam heated evaporators in an ultrahigh vacuum chamber with a base pressure of 3×10^{-9} mbar. Film thickness and alloy composition were determined by the individual calibration of the Fe and Pd deposition rates. The magnetic properties were investigated by observing the polar and longitudinal geometries at room temperature through magneto-optic Kerr effect (MOKE) spectroscopy.[16] For the measurements, the samples were sealed in a chamber with pressure ranging from a vacuum of 1×10^{-5} mbar to H_2 gas at 200 mbar. The MOKE measurement was carried out using a white LED light source. As well know, the penetration depth of visible lights in a metallic surface is above 20 nm, which includes not only the top layer of 2−8 nm FePd, but also the Co(0.3 nm)/[Pt(0.8 nm)/Co(0.3 nm)]$_4$.[17] Therefore, the MOKE measurement includes the signal contributions from the FePd and [Co/Pt]$_n$ layers.

RESULTS AND DISCUSSION

For the MOKE investigation, 2-, 3.5-, 5-, and 8-nm-thick $Fe_{40}Pd_{60}$ alloy films were deposited on Co(0.3 nm)/[Pt(0.8 nm)/Co(0.3 nm)]$_4$/Pt(2 nm)/SiO_2 substrates. The normalized polar and longitudinal MOKE hysteresis loops are shown in Figure 2(a). Measurements were performed at room temperature. The multilayer with a 2-nm-thick FePd capping layer exhibited a tilted loop in the polar direction, and its remanence to saturation magnetization (M_r/M_s) ratio was 0.72. By contrast, its longitudinal signal was weak, revealing that the perpendicular magnetic moment was dominant. The hysteresis loop of the multilayer with a 3.5-nm-thick FePd capping layer became considerably slanted in the polar direction, and a square loop was observed in the longitudinal

https://doi.org/10.1021/acsanm.2c05095
ACS Appl. Nano Mater. 2023, 6, 2784−2790

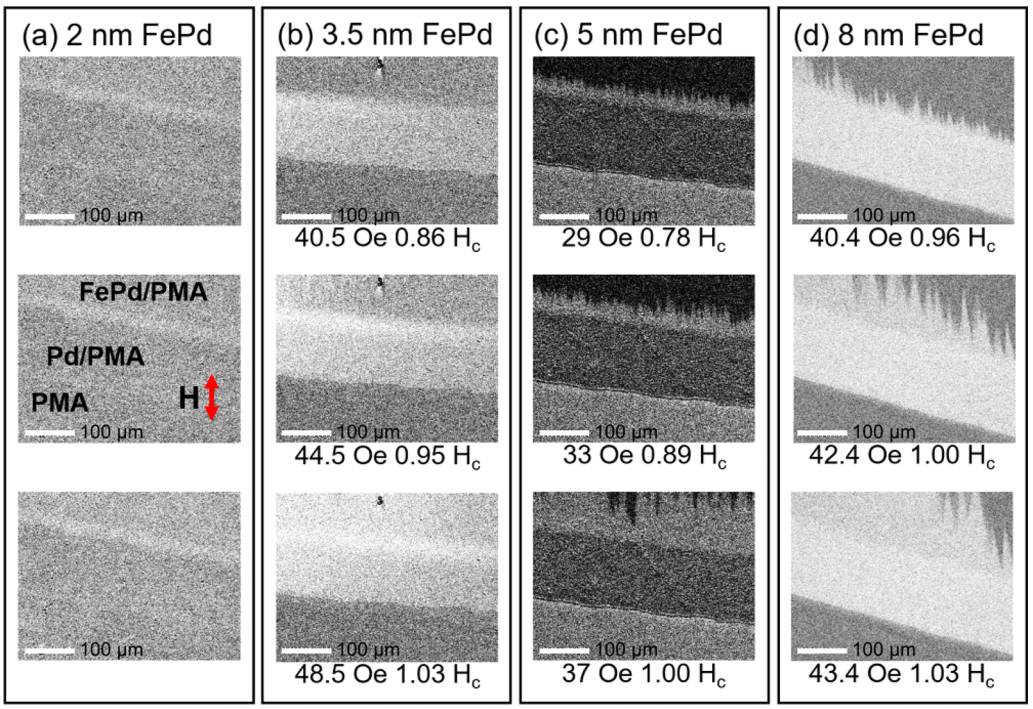

Figure 3. Magnetic-field-dependent longitudinal Kerr images with (a) 2 nm FePd, (b) 3.5 nm FePd, (c) 5 nm FePd, and (d) 8 nm FePd on Co/$[Pt/Co]_4$/Pt. The magnetic field is close to the magnetic coercivity (H_c); thus, the domain evolution can be observed.

direction (canted magnetization). The observable PMA behavior of these two samples was affected by the MPE induced by the Co/Pt bottom layer. However, the hysteresis loops of the multilayers with 5- and 8-nm-thick FePd capping layers were straight lines in the polar direction and square loops in the longitudinal direction, indicating stable IMA.

The magnetic coercivity (H_c) values of the polar and longitudinal hysteresis loops are illustrated in Figure 2(b). Polar and longitudinal H_c decreased and increased monotonically with FePd thickness, respectively. The (a) Polar MOKE hysteresis loops of various PMA multilayers with buffer Pt layers of different thicknesses. The strength of PMA incera ratios of the polar and longitudinal hysteresis loops, which are plotted as a function of FePd thickness, are summarized in Figure 2(c). The M_r/M_s ratio of the polar magnetic hysteresis loops changed from 1 to 0.72 and then to 0 as the FePd thickness increased from 0 to 2 and then to 8 nm, respectively. The multilayer with a 2-nm-thick FePd capping layer had a TMA with a much stronger PMA than the multilayer with a 3.5-nm-thick FePd capping layer and was thus selected for further investigation of the effects of hydrogen exposure, which are discussed in the following sections.

The competition between the FePd-IMA and the Co/Pt-PMA causes the thickness-dependent SRT to alter from a polar to a longitudinal direction as the thickness of the FePd capping layer increases, as shown in Figure 2. Similar thickness-dependent SRT behavior has been reported in magnetic thin film multilayers of various compositions, including Fe/Pd(001)[18] and $Co_{50}Pd_{50}/Al_2O_3(0001)$.[19] SRT behavior is usually dominated by the competition between the surface/interface-contributed PMA and the IMA; thus, the critical thickness for SRT is determined by the intrinsic surface/interface-contributed PMA and is usually difficult to change. Magnetic structures with more sophisticated designs are required to manipulate SRT behavior or control the TMA state.

In the present study, only the longitudinal signal was observed in the multilayers with 5- and 8-nm-thick FePd capping layers; this finding implies that the magnetization of the PMA layer, which changed from the surface normal direction to the in-plane direction, was dominated by the FePd cap. This observation provides an alternative method to reorient the easy direction of PMA-magnetization through the capping effect of FePd. In particular, the TMA state can be achieved by fabricating the sample with a FePd layer that has a thickness that is within the critical region for SRT.

Magnetic-field-dependent Kerr images of the FePd alloy films measured in the longitudinal direction under a vacuum are shown in Figure 3 for film thicknesses of (a) 2 nm, (b) 3.5 nm, (c) 5 nm, and (d) 8 nm. The images were taken over the same area size (400 × 300 μm^2). Three regions (FePd/PMA, Pd/PMA, and pristine PMA) were recorded simultaneously for comparison, as shown in Figure 3(a). As the applied magnetic field became close to the H_c value, the magnetic domain should appear in the Kerr images. The series of Kerr images exhibited different mechanisms of magnetization reversal. As shown in Figure 3(a) and (b), the 2- and-3.5 nm-thick FePd alloy films presented no observable domain structure; only the grayscale of the Kerr images gradually and continuously became brighter with the increasing magnetic field, without observable domain wall motion. The magnetic domain structure was absent for magnetization reversal due to the small nucleation of reverse magnetization. Because the size of the reverse nucleation was below the resolution of the Kerr microscope (approximately 1 μm), only the grayscale change in the Kerr images driven by the magnetic field could be observed.

For the 5- and 8-nm-thick FePd alloy films, zigzag-shaped domains started to appear from the boundary between the

https://doi.org/10.1021/acsanm.2c05095
ACS Appl. Nano Mater. 2023, 6, 2784−2790

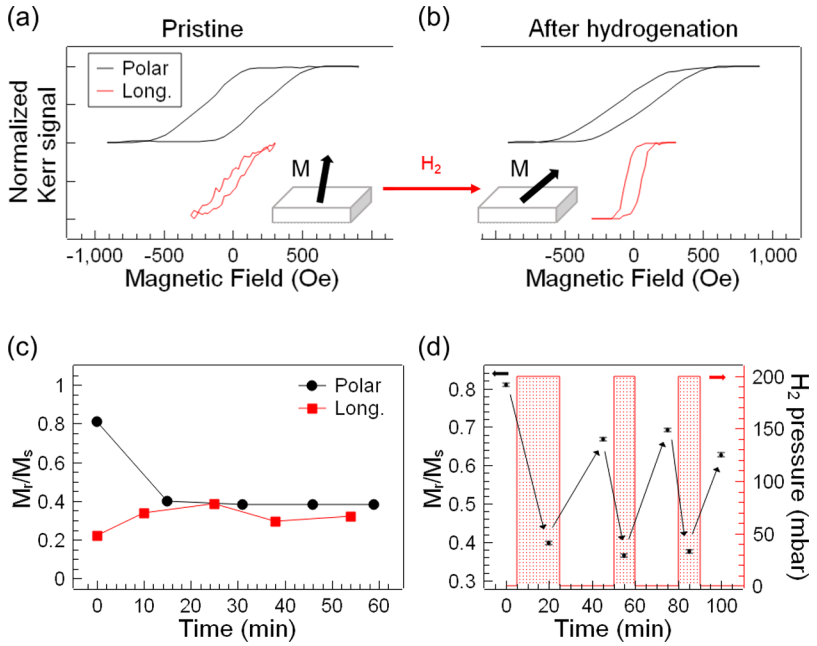

Figure 4. Polar and longitudinal MOKE hysteresis loops of 2 nm FePd/Co (0.3 nm)/[Pt (0.8 nm)/Co (0.3 nm)]$_4$/Pt(2 nm) (a) before, and (b) after hydrogenation. (c) The M_r/M_s ratios of polar and longitudinal Kerr signals are plotted as a function of time in H_2 gas of 200 mbar. (d) The M_r/M_s ratio plotted as a function of time with cyclic changes in gas pressure between a vacuum of 5×10^{-3} mbar and H_2 gas of 200 mbar, which is exhibited by the shadow color corresponding to the right axis.

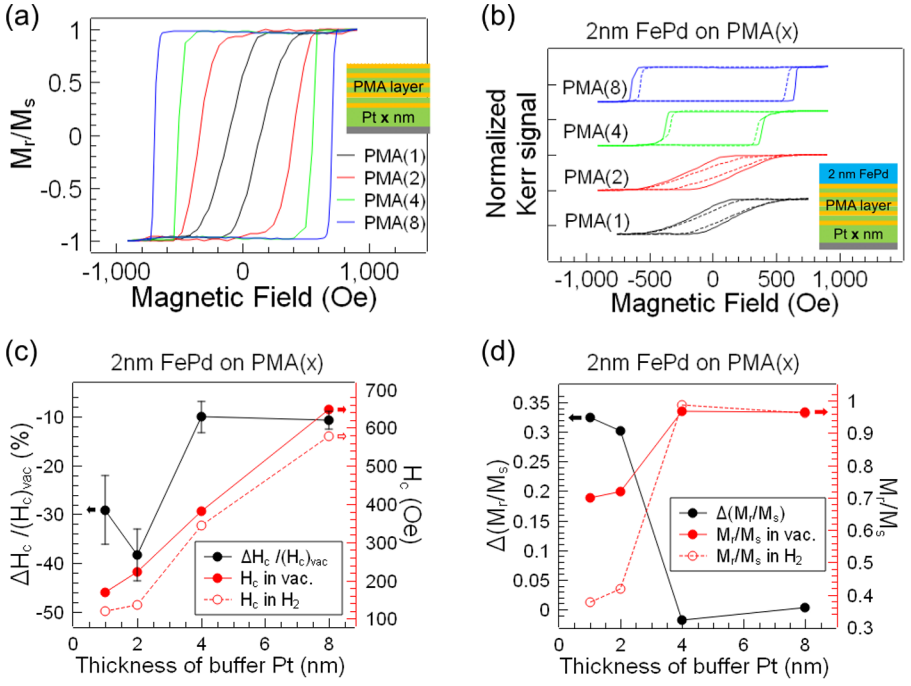

Figure 5. (a) Polar MOKE hysteresis loops of various PMA multilayers with buffer Pt layers of different thicknesses. The strength of PMA incerases as the thickness of the buffer Pt layer increases. (b) Polar MOKE hysteresis loops of 2 nm-thick FePd capped multilayers. The solid and dashed lines were measured before and after exposure to H_2 gas. (c) The magnetic coercivity (H_c) of the 2 nm FePd/PMA multilayers was plotted against time. MOKE measurements began in a vacuum of 5×10^{-3} mbar, then the hydrogen gas pressure was increased to 200 mbar, and finally the sample was exposed to air. (d) Hydrogenation-induced changes of the M_r/M_s ratios (left axis: black solid line). The M_r/M_s ratios measured before (red solid line) and after (red dashed line) H_2 gas exposure are plotted as a function of the buffer Pt thickness.

FePd/PMA and Pd/PMA regions, at which the domain structures were observed with magnetic fields of 0.784 and 0.962 H_c, respectively, as shown in Figure 3(c) and (d). These observations were consistent with the previous MOKE results. With the increasing FePd thickness, the direction of magnetization changed from slightly canted to canted and then to the full in-plane direction. Thus, for the multilayers with 2- and 3.5-nm-thick FePd capping layers, no observable magnetic domain structure was present due to the weak longitudinal magnetic moment and the PMA domination of the nucleation

https://doi.org/10.1021/acsanm.2c05095
ACS Appl. Nano Mater. 2023, 6, 2784−2790

behavior in magnetization reversal. For the multilayers with 5- and 8-nm-thick FePd capping layers, the presence of magnetic domain wall motion, due to the stronger IMA from the increased thickness of the FePd layer, was observed.

To investigate the effect of hydrogenation, the multilayer with a 2-nm-thick FePd capping layer was used because it exhibited TMA behavior with a relatively strong perpendicular component. The polar and longitudinal MOKE hysteresis loops measured in the same region of the sample before and after hydrogenation are shown in Figure 4(a) and (b). After exposure to H_2 gas at a pressure of 200 mbar, the tilting angle of the polar hysteresis loop canted further, and the rectangular longitudinal hysteresis loop was revealed. This observation demonstrated the reorientation of the perpendicular magnetic moment toward the in-plane direction. The M_r/M_s ratios of the polar and longitudinal Kerr signals, plotted as functions of exposure time to hydrogen gas, are shown in Figure 4(c). After exposure to hydrogen gas, the polar M_r/M_s ratio decreased from 0.8 to approximately 0.4, and the longitudinal M_r/M_s ratio increased from 0.2 to 0.4. This finding suggests that the polar and longitudinal signals were saturated within 20 min of exposure to hydrogen gas. The reversibility of the hydrogenation effect on the magnetism of the FePd alloy film was demonstrated according to cyclic changes in gas pressure between a vacuum of 5×10^{-3} mbar and H_2 gas at 200 mbar, as shown in Figure 4(d). These findings indicate that the reversible control of SRT is facilitated by hydrogen absorption and desorption.

To further investigate the thickness-dependent and hydrogen-driven SRT in the FePd/PMA multilayers, we tuned the strength of the PMA by manipulating the thickness of the buffer Pt layer,[20] as shown in Figure 5(a). The H_c values increased from 125 to 755 Oe as the thickness of the Pt buffer layer increased from 1 to 8 nm. These results can be attributed to the improvement in the fcc (111) structure of the Co layer due to the thicker buffer.[21,22] In addition, reduced roughness in the Co/Pt interface enhances interfacial anisotropy, which increases coercivity.[23] The magnetic hysteresis loops became more square as the thickness of the Pt buffer layer increased, which indicates that PMA strength is positively correlated with the thickness of the Pt layer. These results clearly indicate that the PMA is sensitive to the thickness of the buffer Pt layer and is significantly stronger for t_{Pt} = 8 nm than for t_{Pt} = 1 nm.

The MOKE hysteresis loops of the various multilayers with 2-nm-thick FePd capping layers measured before and after exposure to H_2, as denoted by solid and dashed lines, respectively, are shown in Figure 5(b). The H_c values and M_r/M_s ratios of the multilayers with 2-nm-thick FePd capping layers are summarized in Figure 5(c) and (d). In Figure 4(c), as indicated by the solid and dashed red lines, the H_c value increased as the thickness of the Pt buffer increased in both environments. Moreover, the H_c value decreased after exposure to H_2, as indicated by the dashed red line always being below the solid red line. The black line reveals the H_2-induced change in H_c in comparison with pristine H_c, $\Delta H_c/(H_c)_{vac}$. The change in the H_c ratio was the greatest between the 1- and 2-nm-thick FePd capped multilayers (−30% to −40%).

A similar tendency was observed in the M_r/M_s ratio. The M_r/M_s ratios of the multilayers with 2-nm-thick FePd capped layers before and after exposure to H_2 are plotted as a function of buffer Pt thickness in Figure 5(d). The M_r/M_s ratios increased as the Pt buffer thickness increased from 1 to 2 nm and were finally saturated at Pt buffer thicknesses of 4 and 8 nm. The changes of the M_r/M_s ratio induced by hydrogenation decreased dramatically from 0.33 to 0 with the increased thickness of buffer Pt. This finding indicates that the H_2-induced SRT became weaker as the strength of the buffer PMA increased and implies that a stronger buffer PMA layer suppresses H_2-induced SRT behavior.

As shown in Figure 2, the FePd films capped on the multilayer with a 2-nm-thick Pt buffer layer promoted SRT behavior in the FePd thickness range of approximately 3 ± 1 nm. For the multilayer with an 8-nm-thick Pt buffer layer, the SRT behavior was delayed to the 7 ± 1 nm FePd capping layer, as shown in Figure 6(a). It is reasonable to expect that the

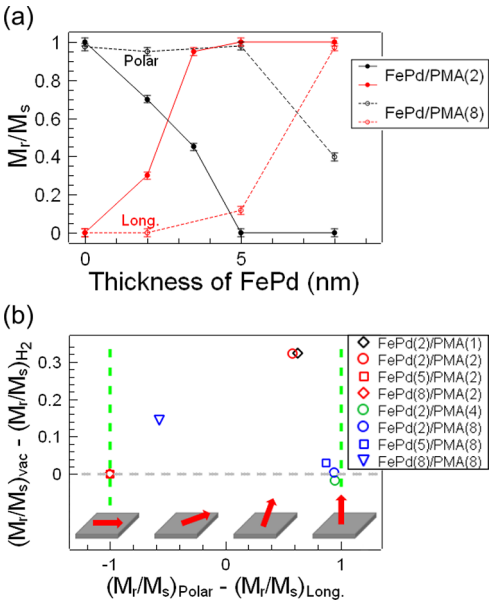

Figure 6. M_r/M_s ratios of polar (black line) and longitudinal (red line) Kerr signals are plotted as a function of FePd thickness deposited on PMA(2) (solid line) and PMA(8) (dashed line). (b) The difference of the M_r/M_s ratios before and after H_2 gas exposure for the polar signals are plotted as a function of the difference between the polar M_r/M_s and longitudinal M_r/M_s ratios in the vacuum.

reorientation of a stronger PMA requires a thicker FePd capping layer, which provides a larger shape-induced IMA. In Figure 6(b), we summarized the hydrogen-induced SRT behavior for various combinations of FePd/PMA by plotting the difference between the M_r/M_s ratios in a vacuum and in H_2 at 200 mbar as a function of the difference between the pristine polar and longitudinal M_r/M_s ratios. The y-axis, polar $(M_r/M_s)_{vac}-(M_r/M_s)_{H_2}$, indicates the degree of H_2-induced SRT from the perpendicular to in-plane direction. The x-axis, $(M_r/M_s)_{Polar}-(M_r/M_s)_{Long.}$, indicates the canting angle of the pristine magnetism in a vacuum. The x value ranges between −1 and 1, indicating that the magnetization oriented from the full in-plane to canted and then to the perpendicular direction, as illustrated at the bottom of Figure 6(b). If the pristine magnetism is in the full perpendicular or in-plane direction, then almost no H_2-induced SRT is observed; the magnetism is too stable to be modulated by hydrogenation. The H_2-induced SRT occurred clearly with pristine canted magnetization. Hydrogenation of FePd/PMA always favors IMA. For the pristine in-plane magnetization, hydrogenation only results in a more stable IMA. For the pristine FePd/$[Co/Pt]_n$ with a full perpendicular magnetization, the FePd capping layer is

https://doi.org/10.1021/acsanm.2c05095
ACS Appl. Nano Mater. 2023, 6, 2784−2790

dominated by the coupling with the strong PMA bottom layer, rather than by the hydrogenation effect. For the canted magnetism, because the FePd-IMA and $[Co/Pt]_n$-PMA are nearly compensated, the hydrogenation effect thus plays an important role in triggering SRT behavior.

To observe SRT in a magnetic system, a critical parameter is usually required for the modulation of either PMA or IMA, so that the dominance of the total MAE can be switched in between. In this FePd(t-nm)/$[Co/Pt]_n$/Pt(x-nm) system, the IMA was increased by the top FePd thickness; in the contrary, the enhancement of PMA was achieved by the Pt buffer layer. While the PMA of $[Co/Pt]_n$ was fixed, the increase of FePd thickness triggered the SRT from perpendicular to in-plane, as shown in Figure 2. With a relatively strong PMA of $[Co/Pt]_n$, a thicker FePd capping layer is required to switch the magnetism, as shown in Figure 6(a). Besides the thickness-dependent SRT, hydrogen absorption played another critical role to enhance IMA through the hydrogen-mediated charge transfer between Fe and Pd. Accordingly, the hydrogen-enhanced IMA resulted in the SRT, which is reversible upon hydrogen absorption/desorption. By controlling the H_2-pressure, the magnetic transition occurred step by step; i.e., the magnetic hysteresis loops become more and more tilted. Regarding the details of the SRT process, one should think about the dynamics in hydrogen dissociation, diffusion, and bonding to Pd−Fe. The MOKE measurement utilized in this study was carried out on a time scale of around 10−100 s, which allows us to observe the hydrogen-induced SRT within 1 min. Nanosized sample structure with the exposed side surface has been demonstrated to promote the hydrogen effect occurring within a few seconds.

The presence of the FePd capping layer brings about two important impacts on the observation of hydrogen-induced SRT. First, the IMA of FePd film weakens and even changes the PMA of $[Co/Pt]_n$ from perpendicular to in-plane orientation. As shown in Figure 2, 2−3 nm FePd switches the magnetization into a canted state and 5 nm FePd already turned the MAE to in-plane direction. Therefore, the critical thickness of 2 nm FePd was chosen for the detection of the hydrogen effect. Second, FePd is able to dissociate hydrogen molecules and absorbed hydrogen into the volume. The presence of H-content in the FePd film could change both the crystalline structure and the electronic structure. In contrast to pure Pd, the saturated hydrogen concentration drastically decreased to less than 5% atomic ratio in FePd alloy materials and thus the expected modulation of the crystalline lattice is actually negligible. On the other hand, the charge transfer between Co−H−Pd was observed and proposed as the critical key mechanism of the hydrogen-induced sensitive change in MAE. In the previous experiment results of FePd film, the hydrogen absorption enhanced the magnetic coercivity, which means the enhancement of IMA, switching the PMA of $[Co/Pt]_n$ to IMA. According to the two mechanisms brought by the FePd capping layer, the bare $[Co/Pt]_n$ multilayer revealed no observable hydrogen effects due to the robust PMA and lack of catalyzed hydrogen dissociation and absorption.

In Sander et al.'s study, hydrogen-induced reversible SRT was observed in ultrathin Ni films; hydrogen adsorbed on the surface and thus brought about the surface lattice relaxation, leading to the SRT through the change of magneto-elastic anisotropy.[24,25] However, this phenomenon was observed in a UHV system and is far from the application in the ambient environment. In the latest decade, the hydrogen-induced reversible change in magnetism has been studied in many systems, which are mostly correlated with the Pd element for catalyzing the dissociation of hydrogen molecules.[12,13,15,19,21,26,27] Hydrogen absorption into the volume of nanometer-thick CoPd alloy film resulted in considerable change in magnetic coercivity, magnetic anisotropy energy (MAE), magnetic domain revolution, etc. In magnetic systems with small perpendicular MAE or canted MAE, hydrogen-induced SRT from PMA to IMA could possibly be observed. However, in order to extend the material system to general PMA films, like $[Co/Pt]_n$, CoFeB, etc., in this experiment, we combine a hydrogen-sensitive FePd layer with a PMA-$[Co/Pt]_n$ bottom to achieve the H-controlled SRT. The FePd capping layer with suitable thickness can weaken the PMA and thus bring about the high sensitivity of hydrogen-induced SRT. Correspondingly, a similar idea can be applied in other PMA systems for future applications.

In the literature, Co/Pd multilayer system exhibited either IMA or PMA, depending on the thickness of Co and Pd, as well as the period number of the multiyear.[28−30] If instead of FePd, we use Co/Pd multilayer with IMA as the capping layer on Co/Pt multilayer, similar hydrogen-induced SRT could be observed. On the other hand, with suitable film thickness and period number, the Co/Pd multilayer can be designed to display a strong PMA, and thus could be used to replace the Co/Pt underlayer for the hydrogen-controlled SRT.

CONCLUSIONS

In this experiment, a hydrogen-sensitive FePd alloy capping layer was added to a Co/Pt multilayer with the PMA to investigate hydrogen-driven SRT behavior. As the thickness of the FePd capping layer increased, the PMA gradually turned to IMA. The multilayer with a 2-nm-thick FePd capping layer was selected for analysis. The magnetic easy axis became canted, and H_2 absorption induced reversible SRT from the perpendicular to in-plane direction. Moreover, with the increasing thickness of the Pt buffer layer, the PMA of the Co/Pt multilayer became stronger, and a higher critical thickness of FePd was required for the thickness-dependent SRT to IMA. Thus, the combination of a PMA-Co/Pt multilayer with a suitable FePd capping layer can form the canted magnetization, which is especially sensitive for hydrogen-driven reversible SRT. These findings may have valuable application in studies on H_2-sensor or H-migration controlled spintronics.

AUTHOR INFORMATION

Corresponding Authors

Minn-Tsong Lin − *Department of Physics, National Taiwan University, Taipei 10617, Taiwan; Institute of Atomic and Molecular Sciences, Academia Sinica, Taipei 10617, Taiwan; Research Center of Applied Sciences, Academia Sinica, Taipei 11529, Taiwan;* orcid.org/0000-0001-7735-4219; Email: mtlin@phys.ntu.edu.tw

Wen-Chin Lin − *Department of Physics, National Taiwan Normal University, Taipei 11677, Taiwan;* orcid.org/0000-0002-1457-8968; Email: wclin@ntnu.edu.tw

Authors

Kun-Jen Hsueh − *Department of Physics, National Taiwan University, Taipei 10617, Taiwan*

Po-Chun Chang − *Department of Physics, National Taiwan Normal University, Taipei 11677, Taiwan*

https://doi.org/10.1021/acsanm.2c05095
ACS Appl. Nano Mater. 2023, 6, 2784−2790

Li-Jie Liaw − *Department of Physics, National Taiwan Normal University, Taipei 11677, Taiwan;* orcid.org/0000-0002-9077-7686

Alltrin Dhanarajagopal − *Department of Physics, National Taiwan Normal University, Taipei 11677, Taiwan*

Complete contact information is available at: https://pubs.acs.org/10.1021/acsanm.2c05095

Notes

The authors declare no competing financial interest.

■ ACKNOWLEDGMENTS

This study was financially sponsored by Ministry of Science and Technology of Taiwan under Grant no. MOST 111-2112-M-003-012, MOST 111-2124-M-003-002, and MOST 110-2112-M-003-019.

■ REFERENCES

(1) Liu, L.; Lee, O. J.; Gudmundsen, T. J.; Ralph, D. C.; Buhrman, R. A. Current-Induced Switching of Perpendicularly Magnetized Magnetic Layers Using Spin Torque from the Spin Hall Effect. *Phys. Rev. Lett.* **2012**, *109*, 096602.

(2) Miron, I. M.; Garello, G.; Gaudin, K.; Zermatten, P. J.; Costache, M. V.; Auffret, S.; Bandiera, S.; Rodmacq, B.; Schuhl, A.; Gambardella, P. Perpendicular switching of a single ferromagnetic layer induced by in-plane current injection. *Nature* **2011**, *476*, 189−193.

(3) Liu, L.; Pai, C. F.; Li, Y.; Tseng, H. W.; Ralph, D. C.; Buhrman, R. A. Spin-Torque Switching with the Giant Spin Hall Effect of Tantalum. *Science* **2012**, *336*, 555−558.

(4) Cai, K.; Yang, M.; Ju, H.; Wang, S.; Ji, Y.; Li, B.; Edmonds, K. W.; Sheng, Y.; Zhang, B.; Zhang, N.; Liu, S.; Zheng, H.; Wang, K. Electric field control of deterministic current-induced magnetization switching in a hybrid ferromagnetic/ferroelectric structure. *Nat. Mater.* **2017**, *16*, 712−716.

(5) Chen, S.; Yu, J.; Xie, Q.; Zhang, X.; Lin, W.; Liu, L.; Zhou, J.; Shu, X.; Guo, R.; Zhang, Z.; Chen, J. Free Field Electric Switching of Perpendicularly Magnetized Thin Film by Spin Current Gradient. *ACS Appl. Mater. Interfaces* **2019**, *11*, 30446−30452.

(6) Cui, B.; Wu, H.; Li, D.; Razavi, S. A.; Wu, D.; Wong, K. L.; Chang, M.; Gao, M.; Zuo, Y.; Xi, L.; Wang, K. L. Field-Free Spin−Orbit Torque Switching of Perpendicular Magnetization by the Rashba Interface. *ACS Appl. Mater. Interfaces* **2019**, *11*, 39369−39375.

(7) Wu, H.; Nance, J.; Razavi, S. A.; Lujan, D.; Dai, B.; Liu, Y.; He, H.; Cui, B.; Wu, D.; Wong, K.; Sobotkiewich, K.; Li, X.; Carman, G. P.; Wang, K. L. Chiral Symmetry Breaking for Deterministic Switching of Perpendicular Magnetization by Spin−Orbit Torque. *Nano Lett.* **2021**, *21*, 515−521.

(8) Peng, B.; Tang, H.; Cheng, Y.; Zhang, Y.; Qiu, R.; Lu, Q.; Zhou, Z.; Liu, M. Voltage Control of Perpendicular Magnetic Anisotropy in Multiferroic Composite Thin Films under Strong Electric Fields. *ACS Appl. Mater. Interfaces* **2021**, *13*, 61404−61412.

(9) Wu, H.; Zhang, J.; Cui, B.; Razavi, S. A.; Che, X.; Pan, Q.; Wu, D.; Yu, G.; Han, X.; Wang, K. L. Field-free approaches for deterministic spin−orbit torque switching of the perpendicular magnet. *Mater. Futures* **2022**, *1*, 022201.

(10) Liu, L.; Qin, Q.; Lin, W.; Li, C.; Xie, Q.; He, S.; Shu, X.; Zhou, C.; Lim, Z.; Yu, J.; Lu, W.; Li, M.; Yan, X.; Pennycook, S.; Chen, J. Current-induced magnetization switching in all-oxide heterostructures. *Nat. Nanotechnology* **2019**, *14*, 939−944.

(11) Kim, H. J.; Moon, K. W.; Tran, B. X.; Yoon, S.; Kim, C.; Yang, S.; Ha, J. H.; An, K.; Ju, T. S.; Hong, J. I.; Hwang, C. Field-Free Switching of Magnetization by Tilting the Perpendicular Magnetic Anisotropy of Gd/Co Multilayers. *Adv. Funct. Mater.* **2022**, *32*, 2112561.

(12) Chang, C.; Kostylev, M.; Ivanov, E. Metallic spintronic thin film as a hydrogen sensor. *Appl. Phys. Lett.* **2013**, *102*, 142405.

(13) Gerber, A.; Kopnov, G.; Karpovski, M. Hall effect spintronics for gas detection. *Appl. Phys. Lett.* **2017**, *111*, 143505.

(14) Tan, A. J.; Huang, M.; Avci, C. O.; Büttner, F.; Mann, M.; Hu, W.; Mazzoli, C.; Wilkins, S.; Tuller, H. L.; Beach, G. S. D. Magneto-ionic control of magnetism using a solid-state proton pump. *Nat. Mater.* **2019**, *18*, 35−41.

(15) Lin, W. C.; Tsai, C. J.; Wang, B. Y.; Kao, C. H.; Po, W. F. Hydrogenation induced reversible modulation of perpendicular magnetic coercivity in Pd/Co/Pd films. *Appl. Phys. Lett.* **2013**, *102*, 252404.

(16) Hong, J. Y.; Chang, S. H.; Ou Yang, K. H.; Yeh, P. C.; Shiu, H. W.; Chen, C. H.; Chiang, W. C.; Lin, M. T. A multifunctional molecular spintronic platform with magnetoresistive and memristive responses via a self-assembled monolayer. *J. Appl. Phys.* **2019**, *125*, 142905.

(17) Sallam, M. O.; Vandenbosch, G. A. E.; Gielen, G.; Soliman, E. A. Integral equations formulation of plasmonic transmission lines. *Opt. Express* **2014**, *22*, 22388.

(18) Chang, P. C.; Chuang, T. H.; Wei, D. H.; Lin, W. C. Thermally modulated hydrogenation in Fe_xPd_{1-x} alloy films: Temperature-driven peculiar variation of magnetism. *Appl. Phys. Lett.* **2020**, *116*, 102407.

(19) Ueno, T.; Nagira, M.; Tohoda, S.; Tagashira, T.; Kimura, A.; Taniguchi, M.; Sawada, M.; Namatame, H. Spin Reorientation Transition of Fe Ultra-Thin Films on Pd(001) Studied by X-Ray Magnetic Circular Dichroism Spectroscopy. *e-J. Surf. Sci. Nanotechnol.* **2008**, *6*, 246−250.

(20) Chang, P. C.; Chen, Y. C.; Hsu, C. C.; Mudinepalli, V. R.; Chiu, H. C.; Lin, W. C. Hydrogenation-induced reversible spin reorientation transition in $Co_{50}Pd_{50}$ alloy thin films. *J. Alloys Compd.* **2017**, *710*, 37.

(21) Huang, J. C. A.; Chen, M. M.; Lee, C. H.; Wu, T. H.; Wu, J. C.; Fu, C. M. Pt thickness and buffer layer effects on the structure and magnetism of Co/Pt multilayers. *J. Magn. Magn. Mater.* **2002**, *239*, 326.

(22) Mathet, V.; Devolder, T.; Chappert, C.; Ferre, J.; Lemerle, S.; Belliard, L.; Guentherodt, G. Morphology and magnetic properties of Pt/Co/Pt sandwiches grown by argon sputter deposition. *J. Magn. Magn. Mater.* **2003**, *260*, 295.

(23) Wu, T. H.; Huang, J. C. A.; Wu, L. C.; Ye, L. X.; Lu, J. Q. Buffer layer effect on magnetic domain structure and coercivity in epitaxial Co/Pt multilayers. *J. Magn. Magn. Mater.* **1999**, *193*, 136.

(24) Sander, D.; Pan, W.; Ouazi, S.; Kirschner, J. Reversible H-Induced Switching of the Magnetic Easy Axis in Ni = Cu001 Thin Films. *PRL* **2004**, *93*, 247203.

(25) Chen, G.; Ophus, C.; Quintana, A.; Kwon, H.; Won, C.; Ding, H.; Wu, Y.; Schmid, A. K.; Liu, K. Reversible writing/deleting of magnetic skyrmions through hydrogen adsorption/desorption. *Nat. Commun.* **2022**, *13*, 1350.

(26) Maksymov, I. S.; Kostylev, M. Magneto-Electronic Hydrogen Gas Sensors: A Critical Review. *Chemosensors* **2022**, *10*, 49.

(27) Shinde, P. V.; Rout, C. S. Magnetic gas sensing: working principles and recent developments. *Nanoscale Adv.* **2021**, *3*, 1551−1568.

(28) Davydenko, A. V.; Kozlov, A. G.; Stebliy, M. E.; Kolesnikov, A. G.; Sarnavskiy, N. I.; Iliushin, I. G.; Golikov, A. P. Dzyaloshinskii-Moriya interaction and chiral damping effect in symmetric epitaxial Pd/Co/Pd(111) trilayers. *Phys. Rev. B* **2021**, *103*, 094435.

(29) Tudu, B.; Tian, K.; Tiwari, A. Effect of Composition and Thickness on the Perpendicular Magnetic Anisotropy of (Co/Pd) Multilayers. *Sensors* **2017**, *17*, 2743.

(30) Klyukin, K.; Beach, G.; Yildiz, B. Hydrogen tunes magnetic anisotropy by affecting local hybridization at the interface of a ferromagnet with nonmagnetic metals. *Phys. Rev. Mater.* **2020**, *4*, 104416.